

## Ferromagnetic nanocylinders electrodeposited into nanoporous alumina template: A magnetometry and Brillouin light scattering study

S. M. Chérif,<sup>1,a)</sup> Y. Roussigné,<sup>1</sup> A. A. Stashkevich,<sup>1</sup> M. Darques,<sup>2,3</sup> K. Bouziane,<sup>4</sup> and L. Piraux<sup>3</sup>

<sup>1</sup>*LSPM-CNRS, Université Paris13, 93430 Villetaneuse, France*

<sup>2</sup>*Institut Néel-CNRS, (CNRS/UJF), 25 Rue des Martyrs BP 166, 38042 Grenoble, France*

<sup>3</sup>*Institute of Condensed Matter and Nanosciences, Université Catholique de Louvain, Croix du Sud 1, B-1348 Louvain-la-Neuve, Belgium*

<sup>4</sup>*Department of Physics, College of Science, Sultan Qaboos University, P.O. Box 36 Al-Khodh 123, Sultanate of Oman*

(Received 22 December 2010; accepted 5 April 2011; published online 23 May 2011)

The static magnetization experimental behavior of cobalt (Co), Permalloy (Py), and nickel (Ni) nanocylinders is obtained from vibrating sample magnetometry while the dynamic behavior for the Co and Py ones is analyzed by means of Brillouin light scattering spectroscopy. Assuming the presence at remanence of two populations of cylinders with up and down magnetizations and including the dipolar coupling between the cylinders, a single analytical model based on a mean-field approach allowed us to satisfactorily analyze both series of experimental results. The model requires three physical parameters, allowing us to derive the in-plane saturation field, the eigenfrequency in the absence of applied field, and the eigenfrequency at the in-plane saturation field; these parameters enable us to adjust the whole variation of the eigenfrequency versus the applied field. Moreover, the effect of the magnetocrystalline anisotropy on the softening of the frequency in the nonsaturated state is clearly evidenced: it is more pronounced when the magnetocrystalline anisotropy is not vanishing and adds to the shape anisotropy (Co c-axis parallel to the cylinder axis); the softening being weak in the other cases (Co c-axis perpendicular to the cylinder axis or Permalloy). © 2011 American Institute of Physics. [doi:10.1063/1.3587170]

### I. INTRODUCTION

Electrodeposited arrays of ferromagnetic nanocylinders (NCs) have been the subject of intensive experimental and theoretical investigations during the last two decades.<sup>1,2</sup> Interesting magnetic properties have been observed such as giant magnetoresistance<sup>1,3</sup> or spin transfer phenomena.<sup>4,5</sup> Potential applications in data storage devices have also stimulated interest in magnetization reversal in individual cylinders.<sup>6,7</sup> Since the possibility of synthesizing materials with a desirable value of uniaxial magnetic anisotropy oriented along the cylinder axis was possible, this feature makes such structures very attractive for potential applications in microwave devices.<sup>8</sup> Microwave absorption in ferromagnetic NCs excited by a homogeneous external electromagnetic field in a wide frequency range has been analyzed by ferromagnetic resonance (FMR).<sup>9–11</sup> The packing density and the cylinder diameter were shown to be striking parameters for the evaluation of the dipolar interactions between the cylinders.<sup>12</sup> These interactions were modeled according to a mean-field approach, assuming an effective uniaxial anisotropy field oriented parallel to the cylinder axis and proportional to the membrane porosity. Recently, the possibility of adjusting the FMR response of self-biased diluted Co NCs has been shown.<sup>13</sup> Similar results have also been reported for NiFe NCs.<sup>14</sup> The authors proposed an expression for the FMR frequency, pre-

dicting two FMR modes corresponding to two populations of magnetized cylinders with up and down magnetization states, respectively. A double ferromagnetic resonance, below magnetization saturation, has actually been experimentally observed and theoretically confirmed.<sup>15</sup> The study of the magnetic response of such a system is therefore of great interest in order to design microwave devices operating without an external magnetic field.

In this work, the static experimental behavior of cobalt (Co), permalloy (Py, Ni<sub>80</sub>Fe<sub>20</sub>), and nickel (Ni) NCs are obtained from vibrating sample magnetometry (VSM), while the dynamic behavior is investigated in the case of Co and Py using Brillouin light scattering (BLS) spectroscopy measurements, respectively. We show that a single analytical model, based on a mean-field approach and assuming the presence at remanence of two populations of cylinders showing up and down magnetizations, taking into account the dipolar coupling between the cylinders, allowed us to satisfactorily analyze both series of experimental results. The model requires three physical parameters allowing us to derive the in-plane saturation field, the eigenfrequency in the absence of the applied field, and the eigenfrequency at the in-plane saturation field; these parameters enable us to adjust the whole variation of the eigenfrequency versus the in-plane applied field. Moreover, in order to point out the role of the magnetocrystalline anisotropy, two series of Co NCs with the c-axis nominally perpendicular (Co c $\perp$ ) and parallel to the cylinders axis (Co c $\parallel$ ) were investigated and their magnetic behavior compared to the isotropic arrays of Py.

<sup>a)</sup>Author to whom correspondence should be addressed. Electronic mail: cherif@univ-paris13.fr.

## II. SAMPLES AND EXPERIMENTAL TOOLS

We have prepared two-dimensional arrays of large aspect ratio ( $\sim 40$ ) cobalt (Co), Permalloy (Py:  $\text{Ni}_{80}\text{Fe}_{20}$ ), and nickel (Ni) nanocylinders (NCs) 30 nm in diameter and 1.3  $\mu\text{m}$  in length in the following manner.<sup>16</sup> Hexagonally ordered porous  $\text{Al}_2\text{O}_3$  templates were first fabricated from sputtered Al layers on silicon substrates using a two-step electrochemical anodization process<sup>6</sup> and afterward were filled with the ferromagnetic materials by means of electro-deposition using concentrated electrolytes.<sup>4,12,16</sup> The diameter of the pores is 30 nm with a membrane porosity of 3.5% ( $5 \times 10^9$  pores/ $\text{cm}^2$ ). Interestingly, the orientation of the crystallographic  $c$ -axis in cobalt NCs of a hexagonal structure may be adjusted either parallel or perpendicular to the cylinders axis.<sup>16</sup> It should be noted that in the case of the crystalline anisotropy normal to the cylinder's axis its in-plane orientation is random. This can be achieved by carefully tuning the electrodeposition parameters (mainly potential and solution  $\text{pH}$ ). In Fig. 1, we present TEM micrographs and the associated diffraction patterns for 30 nm Co NCs deposited at the same  $\text{pH} = 5.2$  and different deposition rates. The dependence of the hcp  $c$ -axis orientation on the deposition current is evident. At a low deposition rate [Fig. 1(a)], the  $c$ -axis, i.e., the [0001] hexagonal axis, is parallel to the cylinders axis, while at a high deposition rate it is perpendicular [Fig. 1(b)].<sup>16</sup> Note that the structure is kept constant along the whole cylinder length, i.e., no grains having another orientation or structure were observed.

The magnetization of the NC arrays was measured with a DMS 1660 VSM in a magnetic field up to 13.5 kOe applied in-plane (longitudinal configuration, i.e., perpendicular to the cylinder axis) and out-of-plane (polar configuration, i.e., parallel to the cylinder axis). The VSM was calibrated using pure nickel ( $M = 54.9$  emu/g). The dynamic properties of the NCs were studied by means of the BLS technique which constitutes a powerful tool for investigating the magnetic properties of magnetic films.<sup>17,18</sup> In a BLS experiment, a beam of  $\text{Ar}^+$  laser light operating on a single mode of the 514.5 nm line is used as a probe to reveal spin waves which are naturally present in the medium under investigation in the 3–300 GHz spectral frequency range. A 200 mW p-polarized light was focused on the surface of the sample and the scattered light was analyzed by means of a Sandercock-type 3+3 pass tandem Fabry-Pérot interferometer. In the present work,

we used the backscattering geometry so that the value of the wave vector of the probed spin waves is experimentally fixed to the value  $k = (4\pi/\Lambda) \sin(\theta)$ , where  $\Lambda$  denotes the wavelength in air of the laser light and  $\theta$  is the angle of incidence. Moreover, the excited spin waves are studied versus the amplitude of the applied magnetic field up to 10 kOe.

## III. RESULTS AND DISCUSSION

### A. Static magnetic measurements

#### 1. Experimental results

In Fig. 2 we show the hysteresis loops measured in both in-plane and out-of-plane configurations (out-of-plane: H parallel to the cylinder's axis i.e., to the  $z$  axis, in-plane: H perpendicular to the cylinder's axis). The out-of-plane loops enable us to point out the peculiar behavior of the (Co  $c\parallel$ ) sample with respect to the other ones while, as shown below, all the in-plane loops are very similar.

Initially, the (Co  $c\parallel$ ) sample retained a large magnetization after applying a field parallel to the cylinders (out-of-plane loops) as indicated by the large value (0.9) of the squareness,  $S$ , defined as the ratio of the remnant magnetization,  $M_r$ , to the saturation magnetization,  $M_s$ ; the other samples present a small magnetization at remanence ( $S < 0.3$ ). Notice also that the corresponding coercive field,  $H_c$ , is the higher one (2.8 kOe while it is lower than 1 kOe for the other samples). The related values of  $H_c$  and  $S$  are reported in Table I. The magnetic behavior of the samples in this geometry can be explained in terms of conventional reasoning. Qualitatively, within the “macro-spin” model, the coercive field in this configuration is determined entirely by the anisotropy of the sample. At zero field, the direction of the magnetization results from several contributions: magnetocrystalline anisotropy, cylinder shape anisotropy, and dipolar interaction between the cylinders.

In the case of the (Co  $c\parallel$ ) sample, the magnetocrystalline anisotropy and the cylinder shape anisotropy act in the same way: they tend to align the magnetization along the  $z$  direction; the dipolar coupling tending to align the magnetization of the neighboring cylinders antiparallel. In this configuration, the magnetocrystalline anisotropy and the cylinder shape anisotropy overcome the dipolar coupling, thus allowing a large remnant magnetization,  $M_r$ . The obtained cycle is typical of an easy-axis loop. In the case of the (Co  $c\perp$ )

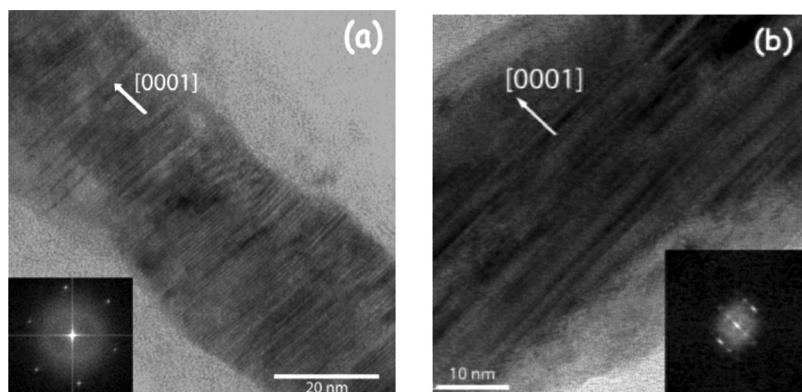


FIG. 1. TEM micrographs of 30 nm Co nanowires electro-deposited at  $\text{pH} = 5.2$  and (a) a low deposition rate (Co  $c\parallel$ ) and (b) a high deposition rate (Co  $c\perp$ ). Reprinted with permission from Appl. Phys. Lett. **86**, 072508 (2005). Copyright 2005 American Institute of Physics.

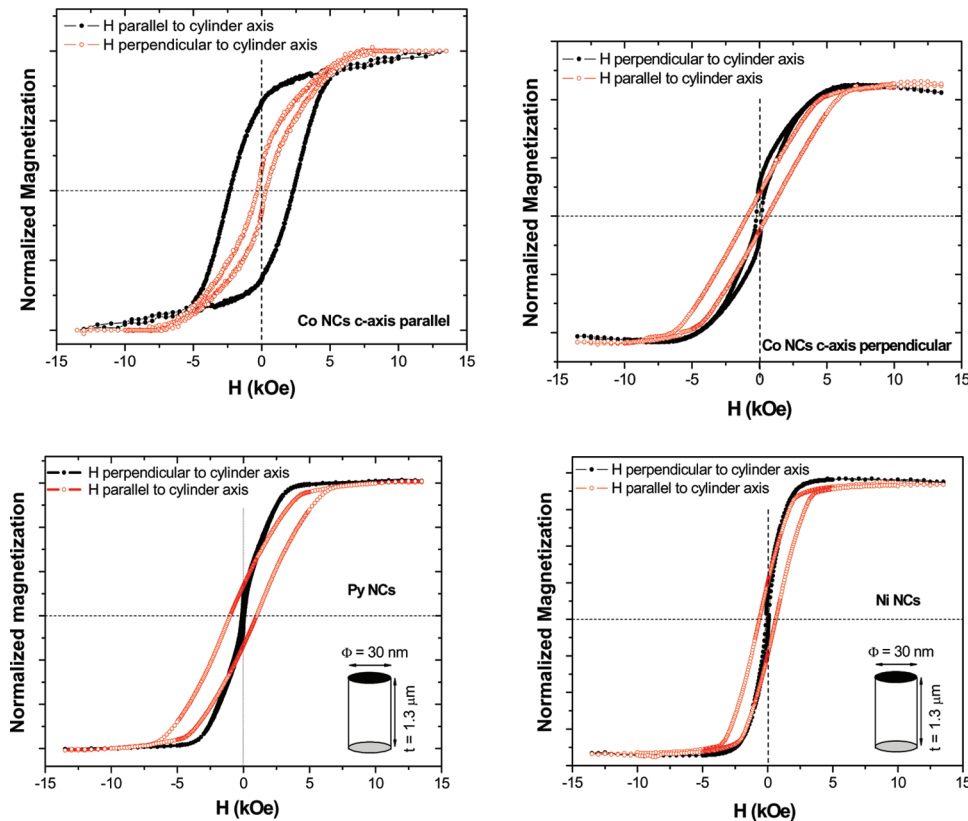


FIG. 2. (Color online) Hysteresis loops measured on (a) (Co c $\parallel$ ), (b) (Co c $\perp$ ), (c) Py, and (d) Ni samples in both the in-plane and out-of-plane configurations ( $\mathbf{H}$  perpendicular or parallel to the cylinder's axis).

sample, the magnetocrystalline anisotropy tends to make the magnetization in plane, thus reducing the cylinder shape anisotropy, leading to smaller values of  $H_c$  and  $M_r$ . Finally, in the absence of a magnetocrystalline contribution (for the cases of Permalloy and nickel), the dipolar coupling can be strong enough to impose an antiparallel configuration and the cycles are less square.

At the same time, the magnetization reversal mechanism cannot be explained by simple reversal schemes. For NCs with large aspect ratio, a reversal proceeding in a nucleation/propagation manner has been theoretically<sup>19,20</sup> and numerically reported via micromagnetic simulations.<sup>21</sup> The study of the coercivity as a function of the NCs diameter reveals a change of the magnetization reversal mechanism from localized quasicohherent nucleation for small diameters to a localized curlinglike nucleation as the diameter exceeds a critical value determined by the exchange length.<sup>22</sup> A study of the magnetic properties of Fe and Ni NCs with diameters smaller than the domain wall width concluded that the reversal

mechanism involves nucleation of a magnetic domain and subsequent propagation of the domain wall along the nanocylinder.<sup>23</sup> That nucleation is triggered near structural defects or at the edge of the NCs. However, for Co wires, a different behavior that is dominated by competition between the shape anisotropy and the temperature-dependent magnetocrystalline anisotropy is observed. The Stoner-Wolfarth model described well the reversal in the case of Co NCs with a diameter of about 3 nm embedded in epitaxial CeO<sub>2</sub> layers while the reversal is localized when the diameter reaches 5 nm.<sup>24</sup> Since the diameters involved are lower than the critical value allowing reversal by curling, the coherent rotation is generally operative. A marked increase in the coercive field characterized the intermediate region between coherent rotation and magnetization curling.<sup>25</sup> The macro-spin concept is especially inadequate in the case when the cylinders are not saturated. More specifically, it emphasizes the importance of the inhomogeneity of the static magnetization, including the presence of the domain structure.

Let us now consider the in-plane applied field hysteresis loops (perpendicular to the cylinders). The magnetization loops look like the ones expected from the usual scheme of a coherent rotation in the hard axis-geometry (Fig. 2). It is also interesting to note that the saturation is reached for higher fields than in the out-of plane configuration.

Indeed, a rigorous numerical approach, however time-consuming, is necessary in order to ensure a reliable and adequate description of the magnetization reversal. However, we show in the next subsection that an analytical approach using understandable physical parameters allows for a good description of the experimental measurements.

TABLE I. Squareness,  $S$ , coercive field,  $H_c$ , and saturation field,  $H_s$ , measured for the various samples with  $\mathbf{H}$  applied parallel or perpendicular to the cylinders.

Samples	H parallel to cylinders			H perpendicular to cylinders		
	$S = M_r/M_s$	$H_c$ (kOe)	$H_s$ (kOe)	$S = M_r/M_s$	$H_c$ (kOe)	$H_s$ (kOe)
(Co c $\parallel$ )	0.9	2.8	5	0.34	0.93	5.5
(Co c $\perp$ )	0.15	0.73	7	0.22	0.2	4.5
Py	0.2	0.9	7	0.15	0.1	3
Ni	0.27	0.63	4	0.15	0.1	2.5

## 2. Analysis of the experimental data

Our experimental results can be analyzed considering two populations of cylinders showing up and down magnetizations as proposed in Refs. 13–15: the  $z$  axis denotes the direction of the cylinders. We assume that when the external field is zero,  $N_1$  cylinders have a magnetization in the direction of increasing  $z$  ( $+\mathbf{e}_z$ ) and  $N_2$  cylinders show a magnetization in the direction of decreasing  $z$  ( $-\mathbf{e}_z$ ). Let us analyze the two investigated experimental configurations.

When the external field  $H$  is applied along the cylinders axis, the loop of the (Co c||) sample presents a large remnant magnetization,  $M_r$ , in contrast with the other loops which present a small value of  $M_r$ . This peculiar behavior means that the individual anisotropy can overcome the dipolar coupling between cylinders only in the (Co c||) sample: this is the only case where nearly all magnetizations can be up-aligned ( $N_2 \ll N_1$ ) when the external field vanishes.

If  $H$  is applied along a direction perpendicular to the cylinder's axis, all loops demonstrate a small remnant magnetization. This means that in these experiments, the antiparallel configuration ( $N_1 \approx N_2$ ) is almost obtained at zero field in all samples i.e., the dipolar coupling makes the magnetizations of two neighboring cylinders antiparallel.

In order to understand the respective behavior we experimentally observed, particularly the remnant state and the saturation in-plane field, we propose the following model. To lighten the formulas, we denote the saturation magnetization  $M$ .

We first assume that the mean individual anisotropy energy of each cylinder reads

$$E_i = -V(aM_z^2 + bM_z^4/M^2), \quad (1)$$

where  $V$  is the volume of one cylinder,  $M_z$  denotes the magnetization component along the cylinder direction,  $a$  and  $b$  are two dimensionless parameters; in the case of an isolated infinite cylinder showing neither magnetocrystalline nor magneto-elastic contributions,  $a = \pi$  and  $b = 0$ ; in the general case, the parameter,  $a$ , is inferior to  $\pi$  but is still positive because the demagnetizing field is usually larger than any other anisotropy field. We regard the arrays of cylinders as a hexagonal lattice. We assume that the dipolar coupling between a cylinder and its neighbors reads,

$$E_c = VcM_{zn}(M_{zp} + M_{zq} + M_{zr} + M_{zs} + M_{zt} + M_{zu}), \quad (2)$$

where  $c$  is a positive dimensionless parameter and  $M_{zn}$  is the magnetization component of the cylinder labeled by  $n$ ; this cylinder is surrounded by the cylinders labeled by  $p, q, r, s, t$ , and  $u$ .

The parameters  $a$ ,  $b$ , and  $c$  will be derived from the analysis of the BLS experiments. However some preliminary indications can be already obtained from the VSM measurements.

In order to deal with the remnant state, we will consider two configurations at zero field:

1. All magnetizations are parallel and are lying along the cylinder direction, yielding a large remnant magnetization when the external field is applied in the direction of the cylinders.

2. The magnetizations of two neighboring cylinders are antiparallel and lying along the cylinders direction, yielding a small remnant magnetization regardless of the direction of the applied field.

In the first case, assuming  $M_z = M \cos(\theta)$ , the total energy reads,

$$E = NV M^2 [-(a \cos^2 \theta + b \cos^4 \theta) + 3c \cos^2 \theta], \quad (3)$$

where  $N$  is the number of cylinders and  $\theta$  is the angle between the magnetization and the  $z$  axis. For small values of  $\theta$ , the energy reads:  $E = NV M^2 [-(a+b) + 3c + (a+2b-3c)\theta^2]$ , thus the configuration  $\theta=0$  is stable only if  $(a+2b-3c) > 0$ .

In the second case, assuming  $M_{z1} = M \cos(\theta)$  and  $M_{z2} = -M \cos(\theta)$ , the total energy reads,

$$E = NV M^2 [-(a \cos^2 \theta + b \cos^4 \theta) - 3c \cos^2 \theta]. \quad (4)$$

For small values of  $\theta$ , the energy reads:  $E = NV M^2 [-(a+b+3c) + (a+2b+3c)\theta^2]$ , thus the antiparallel configuration is valid if  $(a+2b+3c) > 0$ . Regarding these results, we expect that the condition  $(a+2b-3c) > 0$  is fulfilled only in the case of the (Co c||) sample while the condition  $(a+2b+3c) > 0$  should be valid for all samples. We will show further that these conditions are actually realized.

Let us now derive the saturating field when the external field is applied in the plane of the sample, i.e., perpendicular to the cylinder's axis. The  $x$  axis denotes the direction of the in-plane applied field,  $H$ . The initial configuration is antiparallel ( $N_1 = N_2$ ). Let  $(X_1, 0, Z_1)$  be the components of the initially up magnetization (i.e., if  $H=0$ , then  $X_1=0$  and  $Z_1=M$ ). Let  $(X_2, 0, Z_2)$  be the components of the initially down magnetization (i.e., if  $H=0$ , then  $X_2=0$  and  $Z_2=-M$ ).

The total energy reads,

$$E = V(N/2) [-H(X_1 + X_2) - a(Z_1^2 + Z_2^2) - b(Z_1^4 + Z_2^4)/M^2 + 6cZ_1Z_2]. \quad (5)$$

The equilibrium conditions read,

$$\mathbf{H}_1 = H\mathbf{e}_x + (2aZ_1 + 4bZ_1^3/M^2 - 6cZ_2)\mathbf{e}_z \text{ is collinear to}$$

$$\mathbf{M}_1 = X_1\mathbf{e}_x + Z_1\mathbf{e}_z,$$

$$\mathbf{H}_2 = H\mathbf{e}_x + (2aZ_2 + 4bZ_2^3/M^2 - 6cZ_1)\mathbf{e}_z \text{ is collinear to}$$

$$\mathbf{M}_2 = X_2\mathbf{e}_x + Z_2\mathbf{e}_z. \quad (6)$$

These conditions are fulfilled when, respectively,  $X_1 = X_2 = X$ ,  $Z_1 = -Z_2 = Z$ ,  $H = \lambda X$ , and  $2aZ + 4bZ^3/M^2 + 6cZ = \lambda Z$ , where  $\lambda = 2a + 4bZ^2/M^2 + 6c$  while  $Z > 0$  and  $\lambda = H/M$  if  $Z = 0$ . The limit  $Z \rightarrow 0$  defines the saturating field,  $H_s = (2a + 6c)M$ . The measured saturation fields enable us to evaluate  $(2a + 6c)$  assuming the usual saturation magnetization values (see Table II). The experimental values agree well with the evaluated ones when the applied field is perpendicular to the cylinder's axis whereas the agreement is less satisfactory for the out-of-plane applied field; this will

TABLE II. Experimental data [ $F(0)$ ,  $F(H_s)$ , and  $H_s$ ] and fitting parameters ( $a, b$ , and  $c$ ) obtained from VSM and BLS measurements.

	Permalloy	(Co $c\perp$ ) sample	(Co $c\parallel$ ) sample
$F_+(0)$ (GHz)	11	13	21
$F_+(H_s)$ (GHz)	10	14	17
$H_s$ (kOe)	3	4	5
$2a$	1.4	0.9	1.3
$4b$	0.8	0.4	1.3
$6c$	2.3	2	2.3

be discussed in the paragraph related to the BLS measurements in this configuration.

In the case of the Co nanocylinders, our results illustrate the important role of the competition between the magneto-crystalline and shape anisotropies on the magnetization reversal process which is in agreement with what has been observed in the literature.<sup>1,24–27</sup> The direction of the easy axis is determined by such competition and the dependence on temperature of the magnetocrystalline anisotropy.<sup>24,25</sup> The resulting effective anisotropy then enters into competition with the dipolar coupling between the NCs.<sup>25,28,29</sup>

## B. Dynamic magnetic measurements

The dynamical properties of the Co and Py samples have been investigated by means of the Brillouin light scattering (BLS) technique. Making use of the magnons excited by stochastic thermal mechanisms it provides access, in a wide range of frequencies (up to 150 GHz), to the full spectrum of spin waves (SW) magnetic excitations, contrary to the FMR (ferromagnetic resonance) based approach. In the latter case, only the SW modes forming nonzero overlap integrals with the external homogeneous microwave field can be excited. Since in our case, the samples were of very low concentration (packing density,  $P$ , being of the order of only 3.5%), the detection of collective SW modes, existing only in a saturated state, was hardly realistic. That is why, in this paper, we have mainly concentrated on the dynamic behavior of the nonsaturated samples. The transition nature of the nonsaturated state makes it much more sensible to the inter-wire dipolar coupling (both static and dynamic), however weak. This leads to pronounced peculiarities in the SW spectra even in highly diluted samples such as ours.

A theoretical description of the SW behavior of the studied systems is not trivial even in the case of a single isolated

cylinder. Considerable theoretical effort has been made to understand the structure of the existing modes. They have been first treated as purely magnetostatic<sup>30,31</sup> and then the dipole exchange nature of the magnetic waves was considered<sup>32,33</sup> however, the analysis was limited to the particular case of purely cylindrical geometry when the external magnetic field and static magnetization are parallel to the cylinder axis. A more general situation, with an arbitrary orientation of the magnetization with respect to the axis of symmetry, was analytically treated by Tartakovskaya.<sup>34</sup> Notice that when the aspect ratio is high enough ( $>20$ ), which is our case, the vertical spin-wave resonances are not taken into account and the theoretical interpretation fully relied upon the azimuthal and radial modes.

In this work, we have adopted the simplified macro-spin model which excludes any magnetic structure within a cylinder, thus allowing us to concentrate on taking into account non-trivial features resulting from the interplay of static and dynamic dipolar interactions between two major “cylinder populations,” along with those within each “cylinder population.”

### 1. BLS measurements while the external field is applied perpendicular to the cylinders

In Fig. 3 we show a typical BLS spectrum in the case of a magnetic field,  $H$ , applied perpendicular to the NC’s axis for a large (left panel) and a low (right panel)  $H$ , for cobalt NCs with a  $c$ -axis parallel to the NC’s axis (the angle of incidence was equal to  $45^\circ$ ). The inelastic scattering by magnetic modes gives rise to very broad lines which are probably associated with several azimuthal or radial modes<sup>35</sup> that we are not able to resolve experimentally. Thus we show the average position of the broad lines.

The spin wave frequencies were studied as a function of the magnetic field. When the applied field is perpendicular to the cylinder’s axis, there are typically two phases of spin wave behavior, corresponding to the applied field being less than or greater than a critical value related to the effective anisotropy field (Fig. 4). For an infinite isolated cylinder the effective field of perpendicular uniaxial shape anisotropy,  $H_s$ , is equal to  $2\pi M_s$ , typically 8.8, 5, and 3 kOe for a Co, Py, and Ni cylinder, respectively. To take account the inter-NCs dipolar interactions, an effective anisotropy,  $H_s^{dip} = H_s - 6\pi P M_s$ , where  $P$  is the packing density of the cylinders, has been introduced.<sup>16</sup> Thus for  $P=0$ ,  $H_s^{dip}$  is equal to its value in an individual cylinder and for  $P=1$ , to its value for a continuous film. As

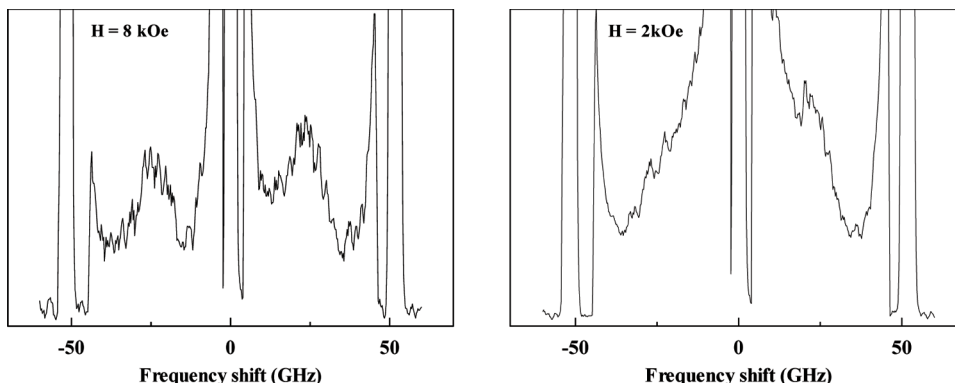


FIG. 3. Cobalt NCs with a  $c$ -axis parallel to the wire axis, and BLS spectrum in the saturated regime ( $H = 8$  kOe) and in the nonsaturated regime ( $H = 2$  kOe) in the case of a magnetic field,  $H$ , applied perpendicular to the cylinder’s axis (in-plane configuration).

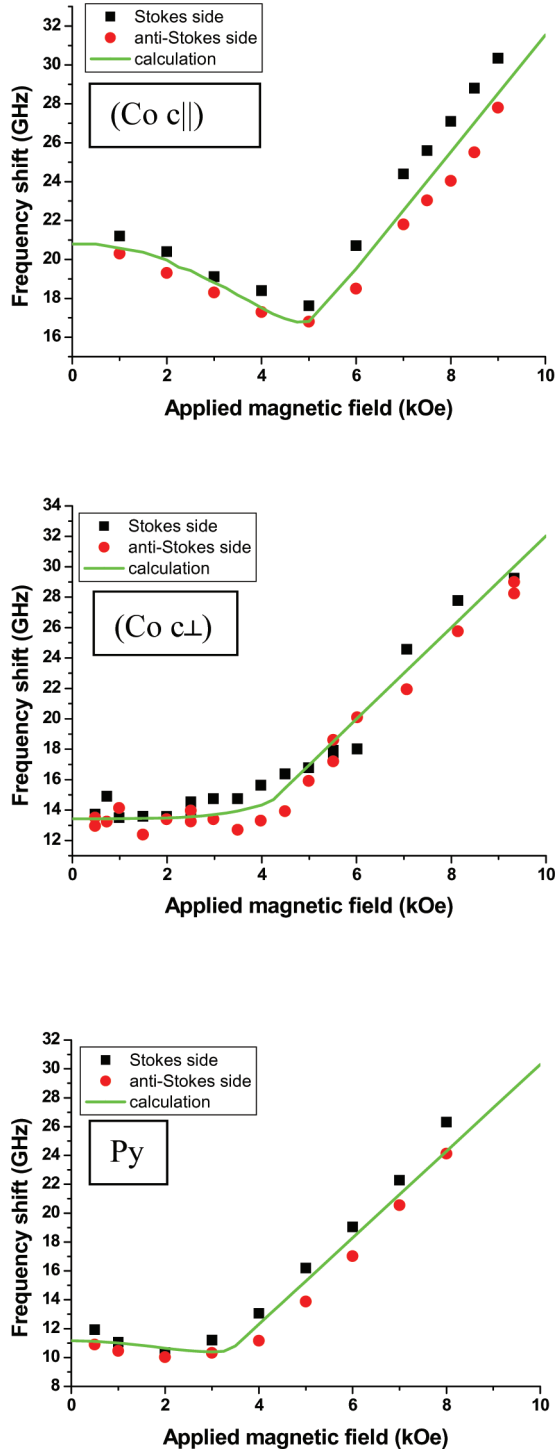


FIG. 4. (Color online) Frequency variation as a function of the external field applied perpendicular to the cylinder's axis. Symbols (experimental Stokes and anti-Stokes data) and continuous line (best fit)

expected, the dipolar interactions contribute to the diminution of the transition field from the out-of-plane nonsaturated state to the in-plane saturated magnetization state ( $H_s$  depends on the material:  $H_s \approx 5, 4,$  and  $3$  kOe for the  $(\text{Co } c\parallel), (\text{Co } c\perp),$  and  $\text{Py}$  samples, respectively). Notice that the effect of the magneto crystalline anisotropy on the softening of the frequency in the nonsaturated state is clearly evident; it is more marked when the magnetocrystalline anisotropy adds to the shape anisotropy ( $\text{Co } c\parallel$  sample); the softening being weak in

the other cases. Also, the zero field frequency,  $F(0)$ , depends on the material. For an applied field,  $H > H_s$ , the frequency varies in a quasilinear manner.

The experimental data are analyzed within the framework of the same model introduced for the discussion of the static measurements. The eigenfrequencies are derived from the Landau-Lifshitz equations

$$\begin{aligned} (i\omega/\gamma) \mathbf{m}_1 &= \mathbf{m}_1 \times \mathbf{H}_1 + \mathbf{M}_1 \times \mathbf{h}_1, \text{ and} \\ (i\omega/\gamma) \mathbf{m}_2 &= \mathbf{m}_2 \times \mathbf{H}_2 + \mathbf{M}_2 \times \mathbf{h}_2, \end{aligned} \quad (7)$$

where  $\omega$  is the angular frequency,  $\gamma$  is the gyromagnetic factor,  $\mathbf{m}_1$  is the dynamic part of the magnetization of the cylinders belonging to the first set (magnetization initially in the direction of increasing  $z$ ),  $\mathbf{h}_1$  is the corresponding dynamic field,  $\mathbf{m}_2$  is the dynamic part of the magnetization of the cylinders belonging to the second set (magnetization initially in the direction of decreasing  $z$ ),  $\mathbf{h}_2$  is the corresponding dynamic field; from the total energy, we derive the effective dynamic fields:

$$\begin{aligned} \mathbf{h}_1 &= \left[ (2a + 12bZ^2/M^2)m_{z1} - 6c m_{z2} \right] \mathbf{e}_z, \\ \mathbf{h}_2 &= \left[ (2a + 12bZ^2/M^2)m_{z2} - 6c m_{z1} \right] \mathbf{e}_z. \end{aligned} \quad (8)$$

The Landau-Lifshitz equations have a nontrivial solution if

$$(\omega/\gamma)^2 = (\lambda Z)^2 + \lambda X^2 \left[ \lambda - (2a + 12bZ^2/M^2) \right] \pm 6c\lambda X^2. \quad (9)$$

The frequency,  $F_+ = \omega_+/2\pi$  is associated with the in-phase mode: the dynamic magnetizations in the two populations of cylinders oscillating in phase.  $F_- = \omega_-/2\pi$  is associated with the out-of-phase mode: the dynamic magnetizations of initially up magnetized cylinders do not oscillate in-phase with the dynamic magnetizations of initially down magnetized ones.

The higher frequency, belonging to the symmetric (or acoustic) mode is used to fit our experimental data because it does not vanish at the saturation field. On the contrary, the asymmetric (optical) lower frequency is no longer in existence when the magnetic field exceeds the critical value of  $H_s$ , which corresponds to the saturation. The fitting curves are displayed in Fig. 4. The best fits are provided using the parameters reported in Table II. The fitting parameters are estimated from the frequency at zero field,  $F_+(0) = (\gamma/2\pi) (2a + 4b + 6c)M$ , the saturating field,  $H_s = (2a + 6c)M$  and the frequency at saturating field,  $F_+(H_s) = (\gamma/2\pi) [12c(2a + 6c)]^{1/2} M$ . We assume  $\gamma/2\pi = 3$  GHz/kOe,  $M$  (Permalloy) =  $800$  emu/cm<sup>3</sup>, and  $M$  (Cobalt) =  $1400$  emu/cm<sup>3</sup>.

Due to its dipolar origin, the parameter,  $c$ , is nearly the same for all samples. The anisotropy field for  $H=0$  reads:  $H_a = (2a + 4b)M$ ; a large remnant magnetization is allowed if this field is greater than the coupling field,  $H_c = 6cM$ , as previously discussed. This condition is fulfilled only for the  $(\text{Co } c\parallel)$  sample:  $2a + 4b = 2.6$ ,  $6c = 2.3$  (see Table II). It is interesting to sort the samples according to the ratio,  $H_a/M = (2a + 4b)$ : the highest ratio [2.6] corresponds to the

(Co c||) sample and the lowest one [1.3] is associated with the (Co c⊥) sample. In the (Co c||) case, the magnetocrystalline contribution acts in the same way as the shape anisotropy, while in the (Co c⊥) case, it acts in the opposite way. For the Permalloy NCs, this ratio (2.2) lies between those of the cobalt NCs. The Permalloy ratio is found to be close to that of the (Co c||) sample. Thus we suspect a strong magneto-elastic contribution to its anisotropy.

## 2. BLS measurements while the external field is applied parallel to the cylinders

Before discussing the BLS experimental data, we consider the expected static states when the external field,  $H$ , is applied along the  $z$  axis. If we assume that all the cylinders are nearly up-magnetized ( $N_1 \gg N_2$ ), then the total energy reads,

$$E = NVM[-H \cos \theta - M(a \cos^2 \theta + b \cos^4 \theta) + 3Mc \cos^2 \theta], \quad (10)$$

where  $\theta$  is the angle between the magnetization and  $\mathbf{e}_z$ . For small values of  $\theta$ , we obtain  $E = NV M \{-H(1 - \theta^2/2) - M[a(1 - \theta^2) + b(1 - 2\theta^2)] + 3Mc(1 - \theta^2)\}$  thus  $\theta = 0$  is a stable state while  $H$  is greater than  $-(2a + 4b - 6c)M$ . According to this calculation, we expect that the reversing field for the (Co c||) sample reads  $(2a + 4b - 6c)M$ , namely 0.42 kOe.

If we assume that half of the cylinders are nearly up-magnetized and the others are nearly down-magnetized ( $N_1 = N_2$ ), then the total energy reads,

$$E = (N/2)VM \times \{-H(\cos \theta_1 - \cos \theta_2) - M[a(\cos^2 \theta_1 + \cos^2 \theta_2) + b(\cos^4 \theta_1 + \cos^4 \theta_2) + 6c \cos \theta_1 \cos \theta_2]\}, \quad (11)$$

where  $\theta_1$  is the angle between the magnetization in the first group of cylinders and  $\mathbf{e}_z$  and where  $\theta_2$  is the angle between the magnetization in the second group of cylinders and  $-\mathbf{e}_z$ . For small values of  $\theta_1$  and  $\theta_2$ , we obtain:

$$E = (N/2)VM \times \{-H(\theta_2^2 - \theta_1^2)/2 - M[a(2 - \theta_1^2 - \theta_2^2) + b(2 - 2\theta_1^2 - 2\theta_2^2) + 6c(1 - \theta_1^2/2 - \theta_2^2/2)]\}, \quad (12)$$

thus  $\theta_1 = \theta_2 = 0$  is a stable state while  $|H| < (2a + 4b + 6c)M$ .

According to this calculation, we expect that the saturating field for the (Co c⊥) sample and the Py sample reads  $(2a + 4b + 6c)M$ , respectively, 4.2 kOe and 3.6 kOe.

The estimations of the reversing field for the (Co c||) sample and the saturating field for the (Co c⊥) sample and Py sample are far below the measured values. This means that in the case of the unsaturated sample submitted to a perpendicular field (i.e., parallel to the cylinders), we cannot assume simple configurations like all magnetizations up ( $N_1/N \approx 1$ ) or half up and half down ( $N_1/N \approx 1/2$ ). Domains are probably present, yielding an intermediate value ( $1/2 < N_1/N < 1$ ).<sup>15</sup> This obviously leads to a peculiar behavior of the frequency variation as discussed in the following text.

In the case of a field applied parallel to the cylinder axis, the behavior of the frequency is not similar to the observed

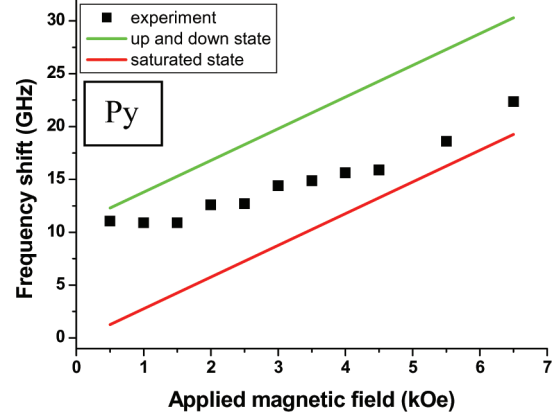


FIG. 5. (Color online) Frequency variation as a function of the external field applied parallel to the cylinders. Symbols (experimental data), the upper curve corresponds to the situation where the two populations of cylinders co-exist: it is the initial situation. The lower curve is the theoretical evolution in the situation where all the magnetic moments are aligned parallel.

one in the perpendicular case. The variation of the frequency versus the amplitude of the magnetic field for the Py cylinders is shown in Fig. 5. The evolution of the frequencies reveals a quasiprogressive evolution from an unsaturated to a saturated regime where the magnetization in all of the cylinders is parallel to the direction of the applied magnetic field. This behavior confirms that at remanence, the cylinders belong to two different families exhibiting magnetization oriented along the positive (negative) direction,  $z$ .

The symbols in Fig. 5 represent the points experimentally obtained. The upper curve corresponds to the situation where the two populations of cylinders co-exist: it is the initial situation; in this case the eigenfrequency reads as  $F = (\gamma/2\pi)[H + (2a + 4b + 6c)M]$ . The lower curve is the theoretical evolution in the situation where all the magnetic moments are aligned; in this case the eigenfrequency reads as  $F = (\gamma/2\pi)[H + (2a + 4b - 6c)M]$ . Because the anisotropy field,  $H_a = (2a + 4b)M = 1.76$  kOe, is lower than the coupling field,  $H_c = 6cM = 1.84$  kOe in the case of Py, the initial state is necessarily the antiparallel configuration; thus, the lower curve could not be reached at zero field. Progressively approaching the saturation for a high enough field, the experimental frequency tends toward the situation (lower curve) where an alignment of all magnetic moments is achieved. This evolution is in agreement with the VSM data where the saturation field in the out-of-plane configuration is about 6 kOe [see Fig. 2 (c)].

## IV. CONCLUSION

Vibrating sample magnetometry (VSM) and Brillouin light scattering (BLS) spectroscopy measurements obtained on large aspect ratio ferromagnetic nanocylinders are analyzed using a single analytical model based on a mean fields approach. Three physical parameters are required to derive the in-plane saturation field, the eigenfrequency in the absence of applied field, and at the in-plane saturation field and to adjust, with good accuracy, the overall variation of the eigenfrequency versus the applied field. Also, the static magnetization behaviors are qualitatively analyzed within the same approach.

## ACKNOWLEDGMENTS

This work has been supported by the Centre de compétences en NanoSciences Ile-de-France (C’Nano IdF) in the framework of the IMADYN Project with the financial support of the Conseil Regional d’Ile-de-France. K.B. is very grateful to the University of Paris 13 for the stay as a visiting Professor.

- <sup>1</sup>A. Fert and L. Piraux, *J. Magn. Magn. Mater.* **200**, 338 (1999).
- <sup>2</sup>D.J. Sellmyer, M. Zheng, and R. Skomski, *J. Phys.: Condens. Matter* **13**, R433 (2001).
- <sup>3</sup>K. Liu, K. Nagodawithana, P. C. Searson, and C. L. Chien, *Phys. Rev. B* **51**, 7381 (1995).
- <sup>4</sup>L. Piraux, K. Renard, R. Guillemet, S. Matefi-Tempfli, M. Matefi-Tempfli, V. Antohe, S. Fusil, K. Bouzouane, and V. Cros, *Nano Lett.* **7**, 2563 (2007).
- <sup>5</sup>N. Bizière, E. Mure, and J.-P. Ansermet, *Phys. Rev. B* **79**, 012404 (2009).
- <sup>6</sup>R. Ferré, K. Ounadjela, J. M. George, L. Piraux, and S. Dubois, *Phys. Rev. B* **56**, 14066 (1997).
- <sup>7</sup>W. Wernsdorfer, B. Doudin, D. Mailly, K. Hasselbach, A. Benoit, J. Meier, J.-Ph. Ansermet, and B. Barbara, *Phys. Rev. Lett.* **77**, 1873 (1996).
- <sup>8</sup>M. Darques, J. De la Torre Medina, L. Piraux, J. Spiegel, and I. Huynen, *J. Magn. Magn. Mater.* **321**, 2055 (2009).
- <sup>9</sup>U. Ebels, J.-L. Duvail, P. E. Wigen, L. Piraux, L. D. Buda, and K. Ounadjela, *Phys. Rev. B* **64**, 144421 (2001).
- <sup>10</sup>C. A. Ramos, M. Vasquez, K. Nielsch, K. Pirola, J. Rivas, R. B. Wehrspohn, M. Tovar, R. D. Sanchez, and U. Gosele, *J. Magn. Magn. Mater.* **272–276**, 1652 (2004).
- <sup>11</sup>O. Yalçın, F. Yildiz, M. Özdemir, B. Aktaş Y. Köseoğlu, M. Bal, and M. T. Tuominen, *J. Magn. Magn. Mater.* **272–276**, 1684 (2004).
- <sup>12</sup>A. Encinas-Oropesa, M. Demand, L. Piraux, I. Huynen, and U. Ebels, *Phys. Rev. B* **63**, 104415 (2001).
- <sup>13</sup>A. Encinas, L. Vila, M. Darques, J.M. George, and L. Piraux, *Nanotechnology* **18**, 065705 (2007).
- <sup>14</sup>X. Kou, X. Fan, H. Zhu, and J. Q. Xiao, *Appl. Phys. Lett.* **94**, 112509 (2009).
- <sup>15</sup>V. Boucher, L.-P. Carignan, T. Kodera, C. Caloz, A. Yelon, and D. Ménard, *Phys. Rev. B* **80**, 224402 (2009).
- <sup>16</sup>M. Darques, L. Piraux, A. Encinas, P. Bayle-Guillemet, A. Popa, and U. Ebels, *Appl. Phys. Lett.* **86**, 072508 (2005).
- <sup>17</sup>S. O. Demokritov and E. Tsybmal, *J. Phys.: Condens Matter* **6**, 7145 (1994).
- <sup>18</sup>M. Belmeguenai, F. Zighem, Y. Roussigné, S. M. Chérif, P. Moch, K. Westerholt, G. Woltersdorf, and G. Bayreuther, *Phys. Rev. B* **79**, 024419 (2009).
- <sup>19</sup>S. Wirth, S. von Molnár, M. Field, and D. D. Awschalom, *J. Appl. Phys.* **85**, 5249 (1999).
- <sup>20</sup>D. Hinzke and U. Nowak, *J. Magn. Magn. Mater.* **221**, 365 (2000).
- <sup>21</sup>R. Hertel and J. Kirschner, *Physica B* **343**, 206 (2004).
- <sup>22</sup>H. Zeng, R. Skomski, L. Menon, Y. Liu, S. Bandyopadhyay, and D. J. Sellmyer, *Phys. Rev. B* **65**, 134426 (2002).
- <sup>23</sup>P.M. Paulus, F. Luis, M. Kröl, G. Schmid, and L. J. de Jongh, *J. Magn. Magn. Mater.* **224**, 180 (2001).
- <sup>24</sup>P. Schio, F. Vidal, Y. Zheng, J. Milano, E. Fonda, D. Demaille, B. Vodungbo, J. Varalda, A. J. A. de Oliveira, and V. H. Etgens, *Phys. Rev. B* **82**, 094436 (2010).
- <sup>25</sup>S. Goolaup, N. Singh, A. O. Adeyeye, V. Ng, and M. B. A. Jalil, *Eur. Phys. J. B* **44**, 259 (2005).
- <sup>26</sup>K. Ounadjela, R. Ferré, L. Louail, J. M. George, J. L. Maurice, L. Piraux, and S. Dubois, *J. Appl. Phys.* **81**, 5455 (1997).
- <sup>27</sup>N. B. Chaure, P. Stamenov, F. M. F. Rhen, and J. M. D. Coey, *J. Magn. Magn. Mater.* **290–291**, 1210 (2005).
- <sup>28</sup>G. J. Strijkers, J. H. J. Dalderop, M. A. A. Broeksteeg, H. J. M. Swagten, and W. J. M. de Jonge, *J. Appl. Phys.* **86**, 249 (1999).
- <sup>29</sup>A. K. M. Bantu, J. Rivas, G. Zaragoza, M. A. Lopez-Quintela, and M. C. Blanco, *J. Appl. Phys.* **89**, 3393 (2001).
- <sup>30</sup>T. Wolfram and T. E. DeWames, *Prog. Surf. Sci.* **2**, 233 (1972).
- <sup>31</sup>S. M. Chérif, Y. Roussigné, and P. Moch, *Phys. Rev. B* **59**, 9482 (1999).
- <sup>32</sup>R. Arias and D. L. Mills, *Phys. Rev. B* **63**, 134439 (2001).
- <sup>33</sup>R. Arias and D. L. Mills, *Phys. Rev. B* **67**, 094423 (2003).
- <sup>34</sup>E. V. Tartakovskaya, *Phys. Rev. B* **71**, 180404(R) (2005).
- <sup>35</sup>A. A. Stashkevich, Y. Roussigné, P. Djemia, S. M. Chérif, P. R. Evans, A. P. Murphy, W. R. Hendren, R. Atkinson, R. J. Pollard, A.V. Zayats, G. Chaboussant, F. Ott, *Phys. Rev. B* **80**, 144406 (2009).